Grain boundaries as preferential sites for resistive switching in the HfO_2 resistive random access memory structures

M. Lanza, K. Zhang, M. Porti, M. Nafría, Z. Y. Shen, L. F. Liu, J. F. Kang, D. Gilmer, and G. Bersuker

Citation: Appl. Phys. Lett. **100**, 123508 (2012);
View online: https://doi.org/10.1063/1.3697648
View Table of Contents: http://aip.scitation.org/toc/apl/100/12
Published by the American Institute of Physics

Grain boundaries as preferential sites for resistive switching in the HfO_2 resistive random access memory structures

M. Lanza,[1,a)] K. Zhang,[2] M. Porti,[1] M. Nafría,[1] Z. Y. Shen,[2,a)] L. F. Liu,[3,a)] J. F. Kang,[3] D. Gilmer,[4] and G. Bersuker[4]
[1]*Dept. Enginyeria Electrònica, Universitat Autònoma de Barcelona, Edifici Q, Bellaterra 08193, Spain*
[2]*Key Laboratory for the Physics and Chemistry of Nanodevices, Department of Electronics, Peking University, Beijing 100871, People's Republic of China*
[3]*Institute of Microelectronics, Peking University, Beijing 100871, China*
[4]*SEMATECH, Austin, Texas 78741, USA*

(Received 23 October 2011; accepted 29 February 2012; published online 23 March 2012)

Resistive switching (RS) phenomenon in the HfO_2 dielectric has been indirectly observed at device level in previous studies using metal-insulator-metal structures, but its origin remains unclear. In this work, using the enhanced conductive atomic force microscope (ECAFM), we have been able to obtain *in situ* direct observation of RS with nanometric resolution. The ECAFM measurements reveal that the conductive filaments exhibiting the RS are primarily formed at the grain boundaries, which were shown exhibiting especially low breakdown voltage due to their intrinsic high density of the oxygen vacancies. © *2012 American Institute of Physics*. [http://dx.doi.org/10.1063/1.3697648]

Resistive random access memory (RRAM) technology is one of the most promising for a variety of the information storage applications due to its simple structure, high switching speed, low operating voltage, and excellent scalability.[1–4] The RRAM principle of operation is a change of the resistance between the two electrodes of a metal-insulator-metal (MIM) structure, which is known as resistive switching (RS).[5] To improve performance of these devices, it is essential to provide accurate knowledge about the switching mechanism. Recent studies have shown that the switching mechanism observed in some high-k dielectric is based on a conductive filament (CF) through the insulator stack that can be created/destroyed depending on the applied voltage,[6] which shows strong similarities with the current limited reversible dielectric breakdown (BD).[7,8] In this work, the RS phenomenon in the HfO_2 films is studied at the device level using the MIM structures and at nanoscale by using both the conductive atomic force microscopy (CAFM) and the enhanced CAFM (ECAFM).[9] High resolution of these techniques (~10 nm) allow for studying the electrical properties of a single CF and identifying the local dielectric properties assisting the RS phenomenon.

Two sets of samples have been analysed by CAFM. The first set (sample A) consisted of a 10.6 nm thick Hf layer deposited by sputtering (and followed by a 600 °C annealing in O_2 ambient for 30 min to form a HfO_2 dielectric) on a Pt/Ti/SiO_2/Si substrate. Then, a 100 nm thick TiN top electrode was deposited at room temperature using the shadow mask, thus defining MIM capacitors of $100 \times 100\ \mu m^2$. X-ray diffraction measurements show that the HfO_2 layer is polycrystalline with grain sizes in the range of ~130 nm. Moreover, the integrity of the structure after the annealing has been corroborated from cross-sectional transmission electron microscopy images, which also revealed a thickness increase of the deposited Hf layer: from 10 nm (as grown Hf) to 15–17 nm (HfO_2 after annealing). The second set of samples includes a 3 nm thick HfO_2 layer sputtered *in situ* (from a HfO_2 target) onto a 3 nm PVD Zr reactive metal, which was deposited on a PVD TiN metal film (bottom electrode) without a vacuum break. To ensure crystallization of the HfO_2 film, some of the samples were subjected to a 400 °C anneal in the N_2 ambient (sample B1) while others, without annealing, were kept as reference (sample B2). Device level electric tests were performed with the 4156 C semiconductor parameter analyzer (SPA). The local electrical properties of the HfO_2 layer of both sets of samples were studied at the nanoscale (resolution of 10 nm) using CAFM and ECAFM.[9] The CAFM was used to obtain topographic and current maps and the ECAFM was used to obtain large current dynamic range IV curves. Note that the standard CAFM current window is only three orders of magnitude, while the ECAFM can measure up to nine orders of magnitude (from 1 pA to 1 mA), making possible the observation of the set/reset curves. To enable a bipolar RS, the CAFM measurements were performed in the N_2 environment to avoid anodic oxidation when the electrons were injected from the tip.[10] Electrical measurements were also performed on the MIM devices fabricated using both sets of the above stacks.

The set A MIM capacitors show the I-V characteristics typical of a MIM structure during the application of a ramp voltage stress (RVS): the current gradually increased until a dielectric BD, at $V = 5.5$ V in this case, has been reached (the maximum measured current corresponds to the current compliance limit, CL, set by the parametric analyzer), Fig. 1(a) (curve #1). The BD, which location is determined by the weakest (electrically) site in the stressed area[11,12] results in the MIM switching to the Low Resistive State (LRS) (curve #2). After the BD, when a negative bias is applied (curve

a)Authors to whom correspondence should be addressed. Electronic addresses: mario.lanza@uab.cat. Telephone: +34935868463. FAX: +34935812600, zyshen@pku.edu.cn. Telephone: +861062762444. FAX: +861062759444, and lfliu@pku.edu.cn. Telephone: +861062753144. FAX: +861062751789.

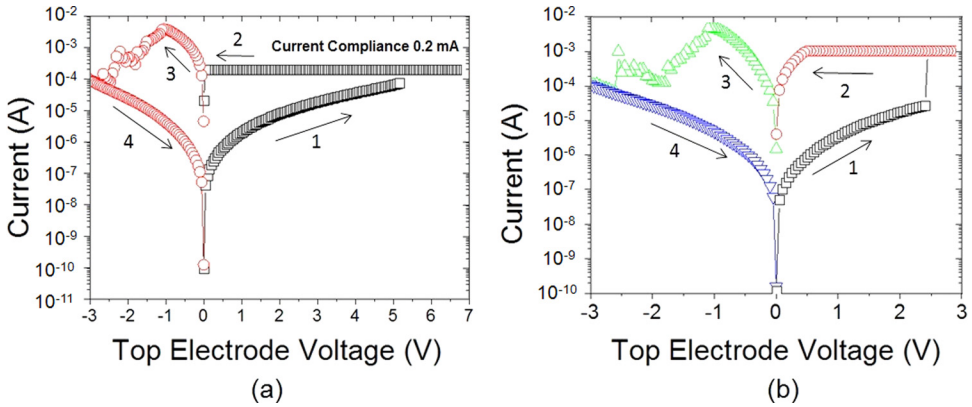

FIG. 1. Forming process and the first reset operation (a) and typical resistive switching behavior (b) observed on the MIM structures of the sample A. Note that the current signal is the sum of the current though each single location of the total stressed area, including CFs and tunneling current through the rest of the gate area.

#3), the conduction is reduced at around −2.5 V, and the device reaches the High Resistive State (HRS) (curve #4). The subsequent positive bias voltage ramp switches the device back to the same LRS (when using the same current compliance limit). The repeatable switching between the LRS and HRS (Fig. 1(b)) indicates a partial recovery of the insulating properties of the HfO_2 dielectric. Note that the current measured by the SPA in Fig. 1 is the sum of the total current through the polarized area, which not only includes the current through different filaments that can coexist in both HRS and LRS, but also the contribution of tunneling current (Fowler Nordheim and/or direct tunneling) at the rest of gate area. Therefore, the observation of RS in these analyses is indirect and there is no way to study the details of the electrical properties of the CFs. To investigate the nature of this reversible conduction phenomenon at a single location, samples A, B1, and B2 have also been analysed at the nanoscale using CAFM and ECAFM.

Ramped voltages have been applied by the CAFM tip on the HfO_2 layer at different locations of the sample A (24 sites), B1 (21 sites), and B2 (20 sites). In sample A (polycrystalline), the *in situ* recorded I-V curves clearly show two different behaviors (Fig. 2(a)). Most of the I-V curves (21 locations) show larger forming voltages (Fig. 2(a), squares), while the others (only 3 locations) exhibit a lower BD voltage (Fig. 2(a), circles, $V_{BD} \sim 4$ V), which is comparable to that measured at the devices in Fig. 1(a). After the CF formation, an additional I-V cycling was performed to determine the electrical properties at each location. Only those sites which exhibit lower V_{BD} values in Fig. 1(a) (red circles) demonstrate a typical bipolar RS (Fig. 2(b)) similar to that in the MIM structures (Fig. 1(b)), with comparable magnitudes of the LRS and HRS currents. The sites with larger V_{BD} (most of them) do not show the RS, meaning that an irreversible breakdown is induced by the forming process. Similar ECAFM measurements were performed on multiple sites in sample B1 (polycrystalline) and B2 (amorphous) subjected to the RVS (Figure 2(c)). The sample B1 demonstrates the characteristics similar to those of the sample A: 3 sites experienced BD at small voltages (∼4–6 V, see inset in Fig. 2(c), red circles) while most of the sites (18) exhibited BD at much larger voltages (inset in Fig. 2(c), black squares). On the contrary, the I-V curves measured on the sample B2 (inset in Fig. 2(c), green triangles) are more homogeneous, with high forming voltages comparable to those obtained on the high-V_{BD} sites in sample B1. Finally, as in sample A, only low-V_{BD} locations in sample B1 showed RS (Fig. 2(c), B1_ grain boundary (GB), red solid line) while in the high-V_{BD} locations of sample B1 and all locations of sample B2 (Fig. 2(c), B1_NC&B2, black dotted line, which also showed a high-V_{BD}) the RS was not observed at any of the probed sites. The backward voltage sweep after the forming process revealed that reversible filaments (Fig. 2(c), B1_GB #2) are less conductive than the irreversible ones (Fig. 2(c), B1_NC&B2 #2), indicating that a much harder BD took place at the latter in spite of a similar current compliance

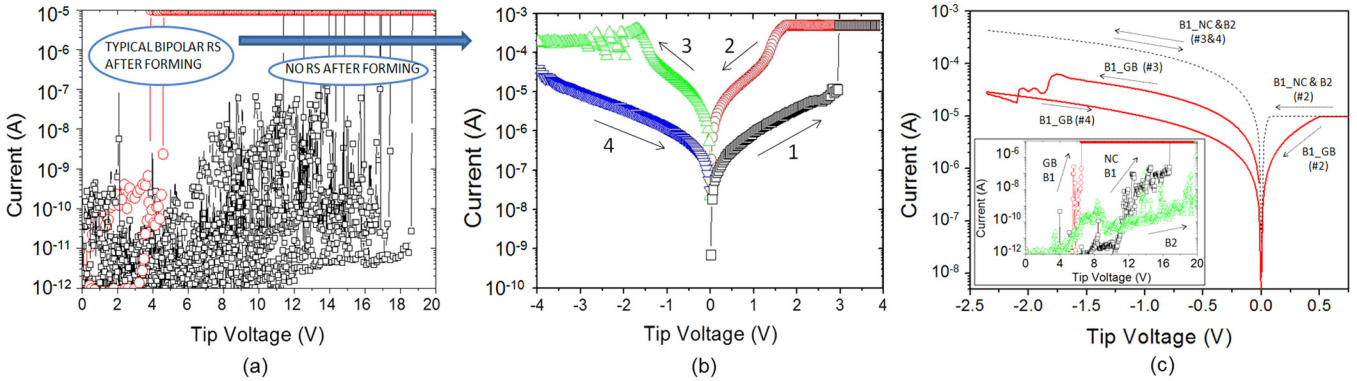

FIG. 2. *In situ* direct observation of RS at each single location using ECAFM. (a) Nanoscale forming processes at 12 different positions of the HfO_2 layer of sample A. (b) Typical bipolar RS behavior obtained in sample A only at those locations where the V_{BD} during the forming process was remarkable lower (red circles in figure a). (c) Typical I-V curves observed in samples B1 and B2 after the forming process (which is shown in the inset). GB, NC, and (#) refer to grain boundary, nanocrystal and ramp number, respectively. For all samples, only in the tests performed at the GBs of polycrystalline stacks (which showed a low-V_{BD} during the forming) the RS was observed.

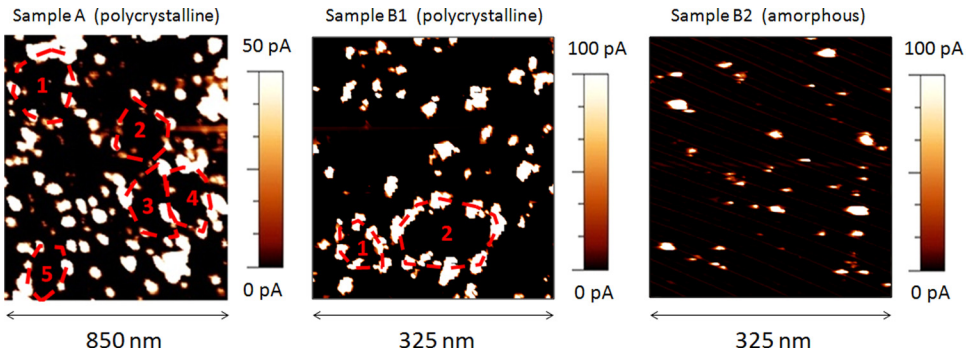

FIG. 3. Current maps obtained when scanning the surface of samples A, B1, and B2 with the tip of the CAFM by applying the minimum voltage to measure current above the noise level in each case. Note that a granular structure is observed in samples A and B1, with GBs being more conductive than grains. Sample B2, which is amorphous, shows a more homogeneous leaky sites distribution.

used in all cases. From these results one can conclude, first, that the RS observed at the device level is controlled by a very small area featuring higher current and sufficiently lower BD voltage values. Moreover, since the major difference between the samples B1 and B2 is the degree of crystallization of the high-k dielectric (from polycrystalline to amorphous), RS is strongly linked to the crystallinity of the HfO_2 film: RS is observed only in the polycrystalline samples A and B1, specifically, in the electrically "weak" sites exhibiting higher currents and lower BD voltages.

Current images of the HfO_2 films in the samples A, B1, and B2 were also collected with the CAFM to identify the RS positions. Fig. 3 presents typical current maps obtained in each samples type. Note that lower currents are measured in sample A. Although the effect of thickness fluctuations of the HfO_2 film cannot be ruled out as a possible origin of leaky sites, the observation of granular structures, which include non-conductive areas (~150 nm, dashed circles) surrounded by the conductive borders, suggests that the conductive borders can be attributed to the grain boundaries, consistent with the earlier reports.[13,14] This assumption is further supported by the fact that the non-conductive grains are in the same size range as the crystal grains measured by XRD. Analysis of the sample B1 (Fig. 3(b), also polycrystalline) yields similar results,[14] however, in these case, the nanocrystals seem to be smaller than in sample A, which should be expected due to smaller thickness of sample B1. Note that in samples A and B1, the probability of probing a GB by the CAFM tip at a randomly selected location, and therefore observing the RS, is much smaller than contacting a grain, which explains a low count for the RS sites in our measurements. On the contrary, in the amorphous sample B2 (where no RS-sites were detected), such granular structure is not observed, while the conduction is much more homogeneous. In this sample, the leaky sites are probably related to dielectric thickness fluctuations and/or presence of randomly distributed defects.

The above results demonstrate that only the polycrystalline HfO_2 dielectrics exhibit the RS phenomenon, which is basically registered at the GBs. Earlier reports have suggested that higher conductivity of the GBs comparing to that of the grains is related to an excess of the oxygen vacancies at the GBs, which were shown to control the trap assisted tunneling current through the dielectric:[15] Higher currents are associated with lower breakdown voltages along the current paths, as observed in Fig. 2(a). Lower forming voltages ensure smaller cross-sections of the created CFs, in part by limiting the overshoot current during the transient BD event, which is too fast to be controlled by the compliance limit set on the electrical tester.[16,17] The CF with a smaller radius is easier to reoxidate during the re-set operation thus enabling a transition to the HRS and subsequent switching.[18]

In conclusion, the RS phenomenon in the amorphous and polycrystalline HfO_2 films has been analyzed at the nanoscale and device levels. The results show strong similarities between the device and nanoscale RS features suggesting that the RS in RRAM devices is controlled by a localized process taking place at the nano-size area of the dielectrics. The local IV curves obtained with the ECAFM point out that RS is only observed at those CF which were formed at sufficiently low voltages at the electrically leaky sites located at the grain boundaries in the polycrystalline samples. This result is consistent with the previously reported high concentration of the oxygen vacancies at the GBs, which are responsible for higher observed leakage currents along the GBs.

This work has been partially supported by the Spanish MICINN (TEC2010-16126), the Generalitat de Catalunya (2009SGR-783 and 2010-BE1-00877), and the National Natural Science Foundation of China (Nos. 60671022 and 60906040).

[1]C. Rohde, B. J. Choi, D. S. Jeong, S. Choi, J. S. Zhao, and C. S. Hwang, Appl. Phys. Lett. **86**, 262907 (2005).
[2]B. J. Choi, S. Choi, K. M. Kim, Y. C. Shin, C. S. Hwang, S. Y. Hwang, S. S. Cho, S. Park, and S. K. Hong, Appl. Phys. Lett. **89**, 012906 (2006).
[3]C. Rossel, G. I. Meijer, D. Bremaud, and D. Widmer, J. Appl. Phys. **90**, 2892 (2001).
[4]I. G. Baek, M. S. Lee, S. Seo, M. J. Lee, D. H. Seo, D. S. Suh, J. C. Park, S. O. Park, H. S. Kim, I. K. Yoo, U. I. Chung, and J. T. Moon, in *Proceedings of the 2004 International Electron Device Meeting, 13–15 December* (IEEE, San Francisco, CA, 2004), p. 587.
[5]G. I. Meijer, Science **319**, 1625 (2008).
[6]M. J. Rozenberg, I. H. Inoue, and M. J. Sanchez, Phys. Rev. Lett. **92**, 178302 (2004).
[7]R. Waser and M. Aono, Nature Mater. **6**(11), 833–840 (2007).
[8]A. Crespo-Yepes, J. Martin-Martinez, R. Rodriguez, M. Nafria, and X. Aymerich, Microelectron. Reliab. **49**(9–11), 1024–1028 (2009).
[9]X. Blasco, M. Nafria, and X. Aymerich, Rev. Sci. Instrum. **76**(1), 016105 (2005).
[10]M. Lanza, M. Porti, M. Nafría, X. Aymerich, E. Wittaker, and B. Hamilton, Rev. Sci. Instrum. **81**, 106110 (2010).
[11]J. Suñé, I. Placencia, N. Barniol, E. Farrés, F. Martín, and X. Aymerich, Thin Solid Films **185**(2), 347–362 (1990).
[12]D. J. DiMaria, E. Cartier, and D. Arnold, J. Appl. Phys. **73**(7), 3367–3384 (1993).
[13]P. Gusev, C. Cabral, Jr., M. Copel, C. D'Emic, and M. Gribelyuk, Microelectron. Eng. **69**(2–4), 145–151 (2003).
[14]V. Iglesias, M. Porti, M. Nafría, X. Aymerich, P. Dudek, T. Schroeder, and G. Bersuker, Appl. Phys. Lett. **97**, 262906 (2010).

[15]G. Bersuker, J. Yum, L. Vandelli, A. Padovani, L. Larcher, V. Iglesias, M. Porti, M. Nafría, K. McKenna A. Shluger, P. Kirsch, and R. Jammy, Solid State Electron. **65–66**, 146–150 (2011).
[16]D. C. Gilmer, G. Bersuker, H.-Y. Park, B. Butcher, W. Wang, P. D. Kirsch, and R. Jammy, in *Proceedings of the Third IEEE International Memory Workshop, 22–25 May* (IEEE, Monterey, CA, 2011), pp. 1–4.
[17]A. Kalantarian, G. Bersuker, D. C. Gilmer, D. Veksler, B. Butcher, A. Padovani, L. Vandelli, L. Larcher, R. Greer, Y. Nishi, and P. D. Kirsch, in *Proceedings of the 42nd IEEE Semiconductor Interface Specialists Conference, Nov 30–Dec 3* (IEEE, Arlington, VA, 2011).
[18]G. Bersuker, D. C. Gilmer, D. Veksler, J. Yum, H. Park, S. Lian, L. Vandelli, A. Padovani, L. Larcher, K. McKenna, A. Shluger, V. Iglesias, M. Porti, M. Nafria, W. Taylor, P. D. Kirsch, and R. Jammy, in *Proceedings of the 2010 International Electron Device Meeting, 6–8 December* (IEEE, San Francisco, CA, 2010), pp. 19.6.1–19.6.4.